Dyes and Pigments 94 (2012) 320–329

Contents lists available at SciVerse ScienceDirect

Dyes and Pigments

journal homepage: www.elsevier.com/locate/dyepig

Bulk heterojunction organic photovoltaic devices based on small molecules featuring pyrrole and carbazole and 2-(4-nitrophenyl)acrylonitrile acceptor segments as donor and fullerene derivatives as acceptor

G.D. Sharma [a,b,*], J.A. Mikroyannidis [c], S.S. Sharma [d], K.R. Justin Thomas [e,**]

[a] Physics Department, Molecular Electronic and Optoelectronic Device Laboratory, JNV University, Jodhpur (Raj.) 342005, India
[b] R & D Center for Science and Engineering, Jaipur Engineering College, Kukas, Jaipur (Raj.), India
[c] Chemical Technology Laboratory, Department of Chemistry, University of Patras, GR-26500 Patras, Greece
[d] Department of Engineering Physics, Govt. Engineering College for Women, Ajmer, Rajasthan, India
[e] Organic Material Research Lab, Department of Chemistry, Indian Institute of Technology, Roorkee 247667, Uttrakhand, India

ARTICLE INFO

Article history:
Received 20 September 2011
Received in revised form
23 November 2011
Accepted 23 December 2011
Available online 1 February 2012

Keywords:
Conjugated small molecules
Pyrrole and carbazole donor units
Bulk heterojunction solar cell
Solvent additives
Nanoscale morphology
Modified PCBM

ABSTRACT

The bulk heterojunction photovoltaic devices based on based on low band gap donor–acceptor (D–A) small molecules, with pyrrole (**P**) and carbazole (**C**) as donor and 2- (4-nitroohenyl) acceptor units as electron donor and (6,6)-phenyl- C_{60} – butyric acid methyl ester (PCBM) and modified PCBM i.e. **F** as electron acceptor were fabricated and characterized. The power conversion efficiency (PCE) of the BHJ organic solar cells based on **P**: PCBM, **C**: PCBM, **P**:**F** and **C**:**F** cast from the THF solvent was 1.20%, 1.46%, 1.90%, 2.06%, respectively. The enhanced PCE for the devices based on **F** as compared to the PCBM may be due to the both increased short circuit current (J_{sc}) and open circuit voltage (V_{oc}). The BHJ organic solar cells based on **P**:**F** and **C**:**F** blends cast from mixed DIO/THF solvent exhibit over all PCE of 2.41% and 3.13%, respectively.

1. Introduction

Recently, the interest in photovoltaic devices based on organic materials has increased because of their potential to deliver low cost solar cells. The thin film of these materials can be solution coated, compatible with flexible substrates and roll to roll fabrication technology, making them attractive for the large scale production [1]. In addition, organic solar cell (OSC) offers the flexibility of chemical tailoring, expanding opportunities for development of new materials. Most of the OSCs consist of a single bulk heterojunction (BHJ) active layer, in which the electron donor (conjugated polymer) and electron acceptor (fullerene derivative) was deposited from a common solvent. As the solvent dries, the electron donor and electron acceptor phases are separated to form nanoscale interpenetrating network with charge separating heterojunction [2]. For the efficient device operation, nanoscale domain size close to the exciton diffusion length is required to permit the excitons to diffuse towards the interface and dissociate into electrons and holes before radiative recombination [2,3]. The thin film blend based on poly (3- hexylthiophene) (P3HT) and [6,6]-phenyl C_{61}-butyric acid methyl ester (PCBM) has been widely explored to fabricate the OSC with power conversion efficiency (PCE) of 4–5% [4]. One of the major problems of OSCs is the lower PCE and smaller photocurrent than that of silicon based solar cell which can be resolved by the development novel materials that can enhance the matching of absorption spectra with the solar spectrum. Considerable attentions have been paid for the development of new materials and morphological structures in order to enhance device performance and indeed impressive PCE of 6–8% have been reported with low bang gap polymers as electron donor and fullerene derivatives as electron acceptor have been reported in recent years [5]. The current certified record PCE is 8.13% [6]. To increase the PCE of OSCs towards the predicted theoretical limits i.e. 10% [7], it is necessary to improve both simultaneously the short circuit current (J_{sc}) and open circuit voltage (V_{oc}). However, the batch to batch variation in the

* Corresponding author. Physics Department, Molecular Electronic and Optoelectronic Device Laboratory, JNV University, Jodhpur (Raj.) 342005, India. Tel.: +91 0291 2720857; fax: +91 0291 2720856.
** Corresponding author.
E-mail address: sharmagd_in@yahoo.com (G.D. Sharma).

0143-7208/$ – see front matter © 2012 Elsevier Ltd. All rights reserved.
doi:10.1016/j.dyepig.2011.12.008

quality of polymers, low reproducibility of average molecular weight, poly-dispersity index (PDI) and difficulty in purification, impose a restriction on their mass production for commercial application [8]. On the other hand, the solution processed small molecule-based donor material for BHJ OSCs are attractive because of their advantages over polymer, which include well defined molecular structure, definite molecular weight and high purity without batch to batch variation [9]. Recently, the small molecule (SM) based bi-layer OSC using thermal deposition has reached the PCE of over 5% which is comparable to polymer based solar cell [10]. However, thermal deposition method can waste large amount of material and also has a limitation in the device fabrication of large area. In recent years, a great amount of research work has been dedicated to develop different type of small molecules, including dendritic oligothiophenes [11], star or X shaped molecules [12], linear analogs with donor–acceptor–donor (D–A–D) structures [13], and other organic dyes [14]. A PCE values up to 4.4% have been reported for the solution processed OSCs with the blend of soluble small organic molecules, as donor materials and fullerene derivative as electron acceptor [14c]. Recently, solution processed OSCs based on a blend of star shaped small molecule and $PC_{71}BM$ afforded a PCE of about 4.3% without any post treatment [12f].

Very recently, our group has synthesized a symmetrical bisazopyrrole (**A**) and the corresponding BF_2-azopyrrole complex (**B**) and used as electron donor for BHJ solar cells. The PCE value of 2.70% and 3.15% for the device based on the **A**:PCBM and **B**:PCBM blends, respectively have been reported [15]. Our group has also synthesized symmetrical small molecules with anthracene and pyrrole segments and achieved PCE of up to 2.42% for the OSC based on these small molecules [16]. Bulk heterojunction photovoltaics based on small molecule based on 2-styryl-5-phenylazo-pyrrole as electron donor and PCBM as electron acceptor have achieved PCE about 2.83% [17]. Moreover, Sharma et al have synthesized a modified PCBM derivative (as shown in Scheme 1), which contains cyanovinylene 4 – nitrophenyl segments. The thin film of **F** shows stronger absorption than PCBM in visible region of solar spectrum [18]

In the present communication, we have investigated the optical and electrochemical properties of two dipolar molecules **P** and **C** having pyrrole or carbazole as bridging donor unit and peripheral 2-(4-nitrophenyl) acrylonitrile acceptor unit. The BHJ devices were fabricated using these small molecules as electron donor along with PCBM and modified PCBM i.e **F** as electron acceptor [18]. The PCE of the devices based on **P**:PCBM and **C**:PCBM blends cast from THF solvent is about 1.20% and 1.46%, respectively, whereas when modified PCBM i.e. **F** is used as the electron acceptor, the PCE for the devices based on **P** and **C** as electron donor has been improved up to 1.90% and 2.06%, under same the conditions. The improved PCE has been attributed to the strong absorption of **F** as compared to PCBM in the wavelength regions below 500 nm, where the both **P** and **C** have minimum absorption. The PCE has been further improved up to 2.41% and 3.13% for the BHJ devices based on the DIO/THF mixed solvent cast **P**:**F** and **C**:**F** blends, respectively.

2. Experimental details

We have used two small molecules **P** and **C** as electron donor and PCBM and modified PCBM i.e **F** as electron acceptor for the present investigation. The chemical structure of these materials is shown in Scheme 1.

We have performed theoretical calculations to understand the electronic structure of the functional materials by using the Gaussian 09W [19] (Revision-A.02) program suite. The geometries of the dyes in gas phase were optimized using density functional theory (DFT) [20] with the hybrid B3LYP [21] density functional and the 6-31G* basis set. All optimized geometries were subjected to vibrational analysis, and characterized as a minimum (no imaginary frequencies). The time-dependent DFT (TD-DFT) [22] at the level of B3LYP/6-31G* was further carried out to determine at least 10 vertical excitations to the excited state of the molecules. The computations in THF were performed by applying polarizable continuum model (PCM) using the integral equation formalism variant (IEFPCM) to describe the electrostatic solute–solvent interactions by the creation of solute cavity via a set of overlapping spheres [23]. The absorption spectra were simulated by using the 10 lowest spin-allowed singlet transitions, mixed Lorentzian–Gaussian lineshape (0.5) and an average full-width at half maximum (3000 cm^{-1}) for all peaks [24].

Electrochemical properties (onset oxidation and reduction potentials) of small molecules were examined with cyclic voltammetry (EDCA instrument). The small molecule was coated onto a glassy carbon electrode, which was used as the working electrode, and immersed in 0.1 M supporting electrolyte Bu_4NPF_6 in acetonitrile solution. Cyclic voltammogram was recorded using Ag/Ag^+ as a reference electrode at a scan rate of 100 mV s^{-1}.

The BHJ photovoltaic devices were fabricated on the pre-cleaned indium tin oxide (ITO) coated glass substrates. First a layer of

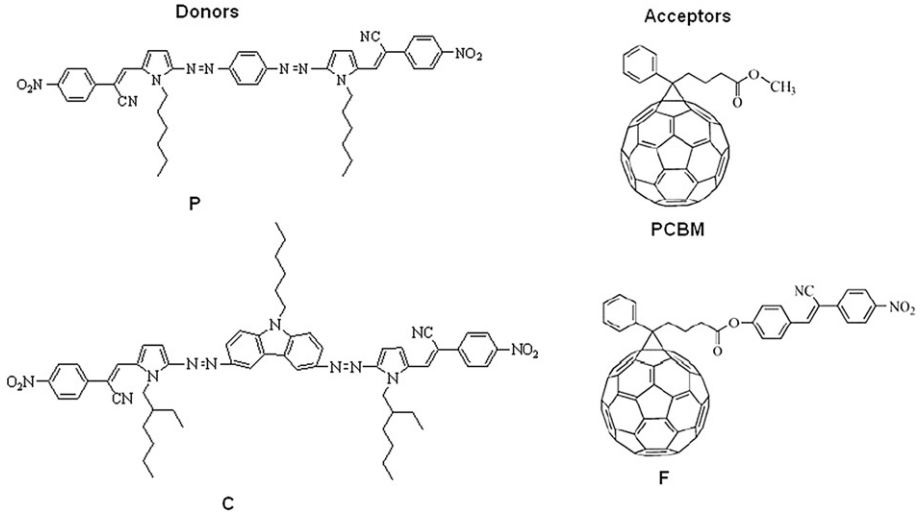

Scheme 1. Chemical structure of **P**, **C**, PCBM and modified PCBM i.e. **F**.

PEDOT:PSS with thickness about 80 nm was deposited by spin casting on ITO coated glass substrate from aqueous solution of poly (3,4–ethylenedioxythiophene): poly (styrenesulfonate) (PEDOT: PSS), at 2000 rpm for 30 s and then dried at 80 °C for 20 min in air. A blend of **P** or **C** and PCBM or **F** (1:1 w/w) in various solvents (i.e. THF or DIO/THF mixed solvent) was stirred for 1 h and then spin coated (1500 for 30 s) on the top of PEDOT:PSS layer. The thickness of the active layer was about 90 nm. The device was completed by depositing 80 nm thin layer of aluminum (Al) at the pressure less than 10^{-5} Torr. The effective active area of the device was 10 mm^2. We have also prepared the devices having structure ITO/ PEDOT:PSS/**P** or **C**/Al to get information about the electrical properties of the **P** and **C**.

The crystallinity of the films was studied using a X-ray diffraction technique (Panalytical make USA) having CuK_α, as radiation source of wavelength $\lambda = 1.5405$ Å with a film coated on glass substrate.

The current–voltage (J–V) measurement of the devices in dark as well under illumination was carried out on a computer controlled Keithley 238 source meter. A xenon light source was used to give an irradiance of 100 mW/cm^2 (equivalent to AM1.5) at the surface of the device.

3. Results and discussion

3.1. Optical and electrochemical properties

To understand the electro-chemical properties of the small molecules i.e. **P** and **C**, we have performed TDDFT calculations. The computed vertical excitation and frontier orbital energies, oscillator strengths for electronic excitations and compositions of vertical transitions in terms of molecular orbitals are listed in Table 1. The electronic distributions observed for selected molecular orbitals contributing significantly to the prominent electronic excitations in these small molecules are presented in Fig. 1. There are two prominent absorptions predicted from the computations for both small molecules. The lower energy absorption corresponds to the HOMO to LUMO transition while the higher energy transition occurs due to a major HOMO − 1 to LUMO + 1 excitation. In **P**, the HOMO is contributed by the central diazenylbenzene segment and the vinylpyrrole unit while the LUMO is delocalized over the entire molecule. On the other hand in **C**, the HOMO is mainly distributed on the diazenylcarbazole and vinyl pyrrole units while the LUMO is contributed by the peripheral 2-(4-nitrophenyl)acrylonitrile unit with some minor representation from pyrrole moiety. From the electronic distributions in the concerned molecular orbitals the lower energy transition occurring in the dye **P** may be described as a π–π* transition and that in **C** as a charge transfer transition from the carbazole and pyrrole moieties to the terminal 2-(4-nitrophenyl) acrylonitrile segment. The oscillator strengths observed for these transitions in the dyes are in agreement with the extended π-delocalization present in the molecular orbitals. The higher energy transition may be assigned as a π–π* transition as the contributing HOMO − 1 and LUMO + 1 orbitals are π-type and spread over the entire molecule.

The electrochemical properties of **P** and **C** were investigated using cyclic voltammetry measurements. The cyclic voltmmograms of these materials are shown in Fig. 2. The values of onset oxidation and reduction potentials versus Ag/Ag^+ are also inserted in Fig. 2. The highest occupied molecular orbital (HOMO) and lowest unoccupied molecular orbital (LUMO) energy levels were estimated from the onset oxidation and reduction potentials, respectively [25], assuming the absolute energy level of Ag/Ag^+ to be 4.7 eV below the vacuum level. The oxidation onset potential of the **P** and **C** was estimated to be 0.60 V and 0.50 V, which corresponds to HOMO energy level of −5.30 eV and −5.20 eV, respectively. The reduction onset potential for **P** and **C** was −1.25 V and −1.45 V, respectively, which corresponds to LUMO energy level at −3.45 eV and −3.25 eV. The electrochemical band gap of **P** and **C** was about 1.85 eV and 1.95 eV, respectively, which is higher than that for optically estimated band gap. Fig. 3 illustrates a diagram of energy levels of the small molecules as compared to that of PCBM, modified PCBM i.e. **F**, and HOMO level of PEDOT:PSS and work function of aluminum (Al) used in OPV devices. The difference between the LUMO energy level of the small molecules (**P** and **C**) and PCBM (−3.95 eV) or **F** (−3.75 eV) is in the range of 0.35–0.6 eV, which is higher than the exciton binding energy (0.3 eV) of most of the organic semiconductors and also to ensure the efficient electron transfer from the donor to acceptor [26]. The lower HOMO energy level of the organic molecule is also very important for the higher V_{oc} of the OPVs, because the V_{oc} is proportional to the difference between the LUMO level of acceptor and HOMO level of the donor used in the BHJ active layer [7].

The simulated absorption spectra of the **P** and **C** are shown in Fig. 4. The trends observed in the frontier orbital and vertical excitation energies for the two molecules are in agreement with the theoretical prepositions. The replacement of the central core benzene by carbazole leads to dramatic alterations in the electronic properties of the molecules. Firstly the stabilization of the HOMO occurs due to effective electronic delocalization and lowers its energy. Secondly, the enhanced donor strength of carbazole causes a significant electronic interaction with the peripheral 2-(4-nitrophenyl) acrylonitrile acceptor unit and raises the LUMO of the molecules. However, lowering of HOMO and highly placed LUMO in **C** increases the band-gap and shifts the absorption to lower wavelength region when compared to that in **P**.

Table 1
Electronic properties of **P** and **C** obtained from DFT computations using B3LYP/6-31G(d).

Sample	λ_{max}, nm (eV)	Oscillator Strength	Composition	HOMO, eV	LUMO, eV	Band gap, eV	Dipole Moment, Debye
P (air)	640 (1.94)	3.29	HOMO → LUMO (100%)	−5.68	−3.61	2.07	0.647
	411 (3.02)	0.34	HOMO − 1 → LUMO + 1 (82%)				
			HOMO − 4 → LUMO (12%)				
P (THF)	690 (1.80)	3.46	HOMO → LUMO (99%)	−5.49	−3.43	2.06	0.689
	427 (2.90)	0.35	HOMO − 1 → LUMO + 1 (92%)				
C (air)	591 (2.10)	2.49	HOMO → LUMO (99%)	−5.48	−3.13	2.35	14.550
	489 (2.54)	0.99	HOMO − 1 → LUMO + 1 (96%)				
	481 (2.58)	0.47	HOMO − 1 → LUMO (62%)				
			HOMO → LUMO + 1 (33%)				
C (THF)	639 (1.34)	2.87	HOMO → LUMO (99%)	−5.32	−3.06	2.26	19.220
	528 (2.35)	0.38	HOMO − 1 → LUMO (90%)				
	512 (2.42)	0.75	HOMO → LUMO+1 (9%)				
			HOMO − 1 → LUMO + 1 (95%)				

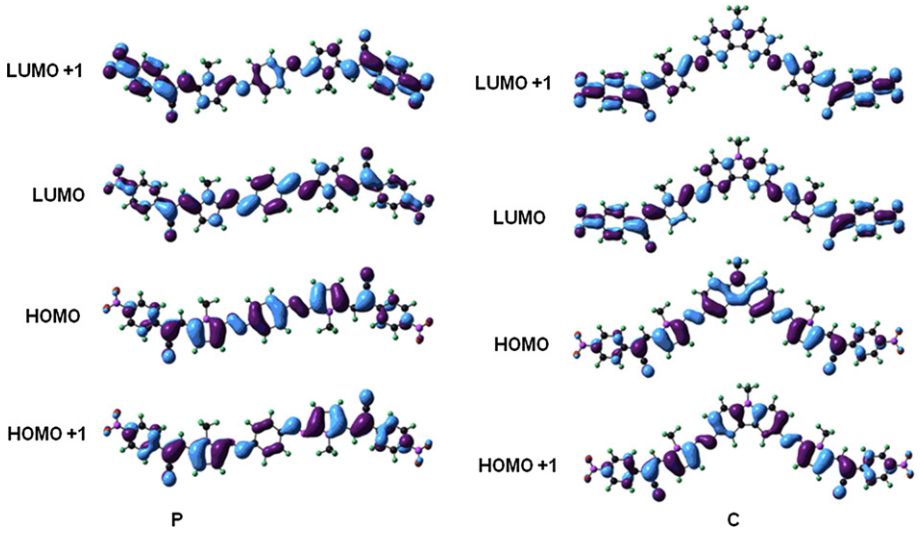

Fig. 1. Electronic distributions observed for the **P** and **C** in selected frontier molecular orbitals.

The absorption spectra of **P** and **C** in thin film form (Fig. 5) show absorption onset at 730 nm and 770 nm, respectively corresponding to optical band gaps of 1.70 eV and 1.62 eV, respectively. The short wavelength absorption peak has been ascribed to a delocalized excitonic $\pi-\pi^*$ transition in the conjugation chains whereas the long wavelength absorption peak attributed to the intra-molecular charge transfer (ICT) between donor and acceptor moieties.

3.2. Electrical properties of small molecules

We have investigated the electrical properties of pristine SMs (i.e. **P** and **C**), using single layer device, to get information about the type of semiconductivity of these materials. Fig. 6 shows the current–voltage (J–V) characteristics of the devices based on **P** or **C** thin film sandwiched between anode (ITO/PEDOT:PSS) and cathode (Al) electrodes in dark, at room temperature. The J–V characteristics of these devices showed the rectification effect, in dark, when a positive potential was applied to the anode with respect to cathode. Since the HOMO level of PEDOT:PSS (5.1 eV) is very close to the HOMO level of both **P** (−5.30 eV) and **C** (−5.20 eV), the anode electrode forms an Ohmic contact for hole injection from anode into the HOMO level of SM. However, the LUMO level of **P** and **C** is −3.45 eV and −3.25 eV, respectively, which is very far from the work function of cathode and forms the Schottky barrier for the electron injection from anode into the LUMO level of SM. Therefore, the rectification observed in the J–V characteristics is due to the formation of the Schottky barrier between the cathode and SM layer, and both **P** and **C** behave as p type organic semiconductor and can used as an electron acceptor for BHJ solar cells.

The charge carrier mobility of the organic semiconductor used as photoactive thin film layer in OSC is also an important factor that influences both the J_{sc} and PCE of the device. The charge carrier mobility in an organic semiconductor film can be estimated from the J–V characteristics in dark using space charge limited current (SCLC) [27]

$$J_{SCLC} = \left(\frac{9}{8}\right)\varepsilon_o\varepsilon_r\mu\left(\frac{V^2}{L^3}\right)$$

where J_{SCLC} is the current density in SCLC region, ε_o is the permittivity of free space, ε_r is the dielectric constant of the material, μ is the charge carrier mobility, V is the applied voltage corrected for the built in voltage (V_{bi}) arising from the difference between the work function of the contacts, and L is the thickness of the organic layer. The hole mobility for **P** and **C** films was estimated by measuring the J–V characteristics (Fig. 7) of the hole only device having structure ITO/PEDOT:PSS/**P** or **C**/Au. The hole mobility estimated from fitting these curves with SCLC model are 5.6×10^{-5} cm^2 V^{-1} s^{-1} and 7.3×10^{-5} cm^2 V^{-1} s^{-1} for **P** and **C**, respectively. Since both SMs have similar chemical structure and the only difference is in their central unit, therefore the difference in hole mobility is due the difference in central unit.

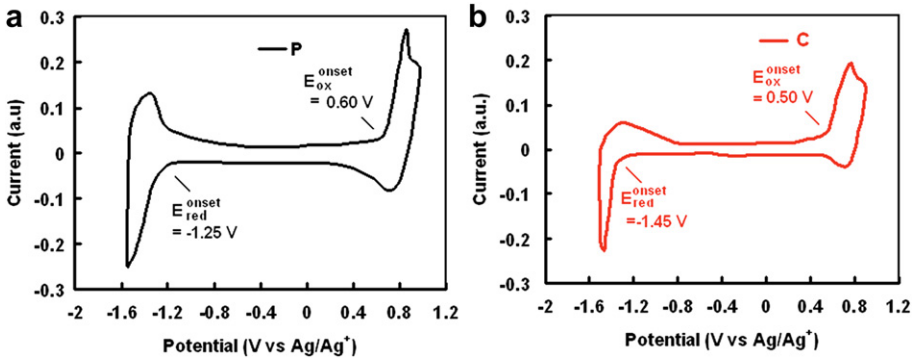

Fig. 2. Cyclic voltammogram of (a) **P** and (b) **C** small molecules at scan rate 100 mV/s.

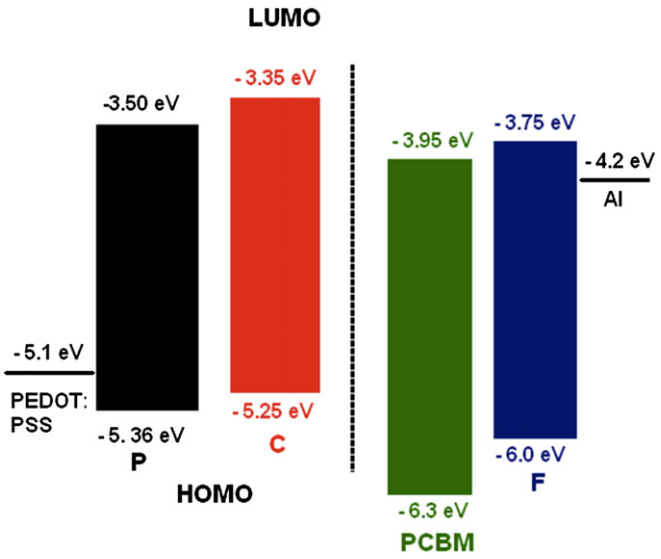

Fig. 3. HOMO and LUMO energy levels of the **P**, **C**, PCBM and **F** and work function of PEDOT:PSS and Al.

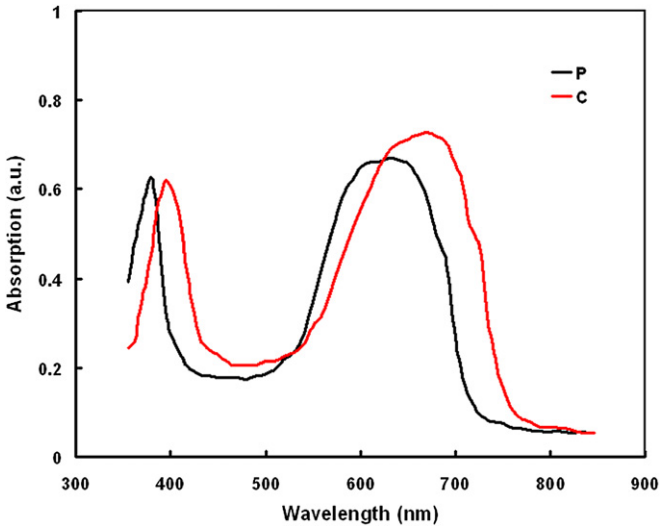

Fig. 5. Optical absorption spectra of **P** and **C** in thin film form cast from THF solvent.

3.3. Photovoltaic properties of BHJ devices

The optical absorption spectra of the **P**:PCBM, **P**:**F**, **C**:PCBM and **C**:**F** blend films cast from the THF solution are shown in Fig. 8. In these spectra, the peak located at the longer wavelength region corresponds to the either **P** or **C** in their respective blends, whereas the peak corresponds to the shorter region attributed to either PCBM or **F**. The broader absorption of the blends based on **F** as electron acceptor as compared to PCBM is due to the strong absorption of **F** in lower wavelength region.

Fig. 9(a) and (b) show the J–V curves of the BHJ OSCs based on the blend of **P**:PCBM, **P**:**F**, **C**:PCBM and **C**:**F** cast from THF solvent, under illumination of AM 1.5, with intensity 100 mW cm^{-2}. The weight ratio of donor: acceptor used in the blend for all devices was 1:1 (w/w). The photovoltaic performance data of the OSCs including open circuit voltage (V_{oc}), short circuit current (J_{sc}), fill factor (FF) and power conversion efficiency (PCE) values are summarized in Table 1. For **P**, the device with PCBM as electron acceptor showed a V_{oc} of 0.87 V, a J_{sc} of 3.6 mA cm^{-2}, and FF of 0.38 that corresponds to a PCE of 1.20%. In comparison to the OSC device based on **F** as electron acceptor exhibited a V_{oc} of 0.96 V, J_{sc} of 4.5 mA cm^{-2}, FF of 0.44 and a PCE of 1.90%. However, the device based on **C**:PCBM showed a V_{oc} of 0.82 V, a J_{sc} of 4.24 mA cm^{-2}, a FF of 0.42, resulting a PCE of 1.46%. In comparison to OSC based on **C**:**F** exhibited a V_{oc} of 0.86 V, a J_{sc} of 5.1 mA cm^{-2}, a FF of 0.46, corresponding to a PCE of 2.06%. The PCE of the OSCs based on **F** as electron acceptor is higher that that for PCBM counterpart which can be ascribed to the stronger absorption of the **F** in visible region, where the PCBM has low absorption [18]. The OSCs based on **C** exhibited better photovoltaic performance, especially the J_{sc} and PCE values, which benefited from the broad absorption (the absorption edge of the **C** film is red shifted to that of **P** film) as compared to **P**. Since the J_{sc} mainly depends on: (i) the number of photogenerated excitons, (ii) their subsequent dissociation into free electrons and holes at D/A interface, and (iii) collection of electron

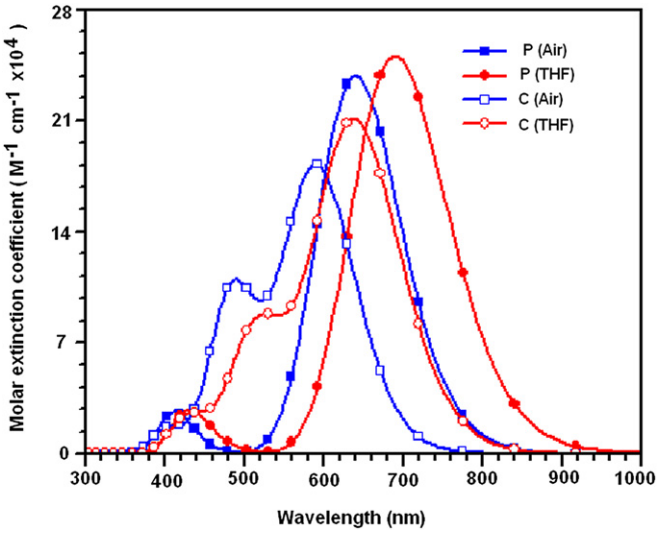

Fig. 4. Simulated (fwhm = 3000 cm^{-1}) absorption spectra of the **P** and **C** small molecules.

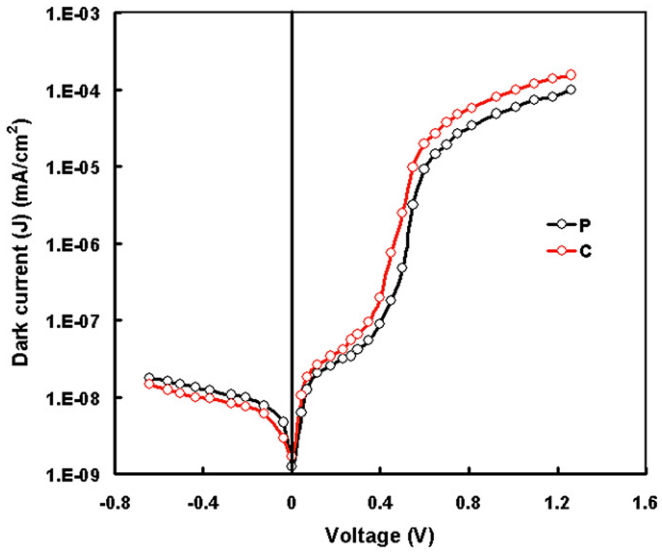

Fig. 6. Current–voltage characteristics of the ITO/PEDOT:PSS/**P** or **C**/Al in dark at room temperature.

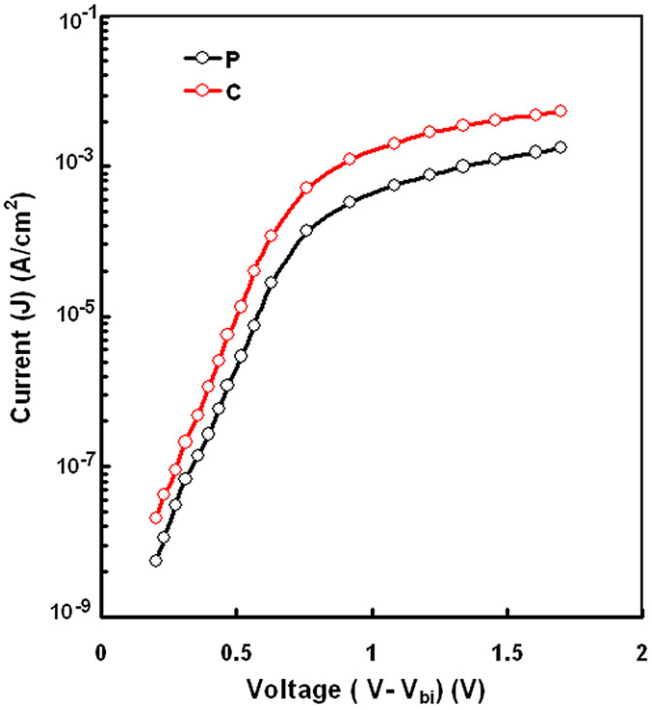

Fig. 7. Variation of current (J) with effective applied voltage (V−V_{bi}) for ITO/PEDOT:PSS/**P** or **C**/Au devices in dark at room temperature.

and hole to cathode and anode, respectively. The broader absorption band of **C** as compared to that of **P**, leads to better light harvesting, resulting more exciton generation in the active layer consists of **C**. The higher hole mobility for **C** also results better hole collection by the anode. These two combined effects generate higher J_{sc} for the OSC based on **C** thereby leading to higher PCE. The HOMO energy level of the **P** is slightly deeper in comparison to that of **C**, which benefits to the higher V_{oc} for the OSCs based on **C**, since the V_{oc} for the BHJ OSCs is proportional to the difference in HOMO energy level of donor and LUMO energy level of acceptor components used in the BHJ active layer.

The values of incident photon to current efficiency have been estimated using following expression:

$$\mathrm{IPCE}(\%) = 1240 J_{sc}/\lambda P_{in}$$

where P_{in} (W/m^2) and λ (nm) are the illumination intensity and wavelength of monochromatic light, respectively. The IPCE spectra of devices based on the blends are shown in Fig. 10(a) and (b). It can be seen from these figures that the IPCE spectra of these devices closely resemble with the absorption spectra of the blends used for the respective devices. The value of IPCE for the devices based on **C** as electron donor is higher than that for the devices based on **P**, which is consistent with the value of J_{sc}. It is observed that the values of IPCE in shorter wavelength region for the devices based on **F** as electron acceptor is higher than that for PCBM based devices. The higher value of IPCE for the devices based on the **F** as acceptor is attributed to the photocurrent contribution due to the exciton generation in the **F** component of the blends and their subsequent dissociation into free charge carriers at the D/A interfaces formed between the donor and acceptor in the BHJ active layer. We assume that the increased value of J_{sc} and thereby IPCE is attributed to the absorption in the wavelength range 350–600 nm, arising from **F**. The replacement of PCBM by the modified PCBM i.e. **F** shows a wide absorption band at shorter wavelength region, which causes an increased PCE of the devices.

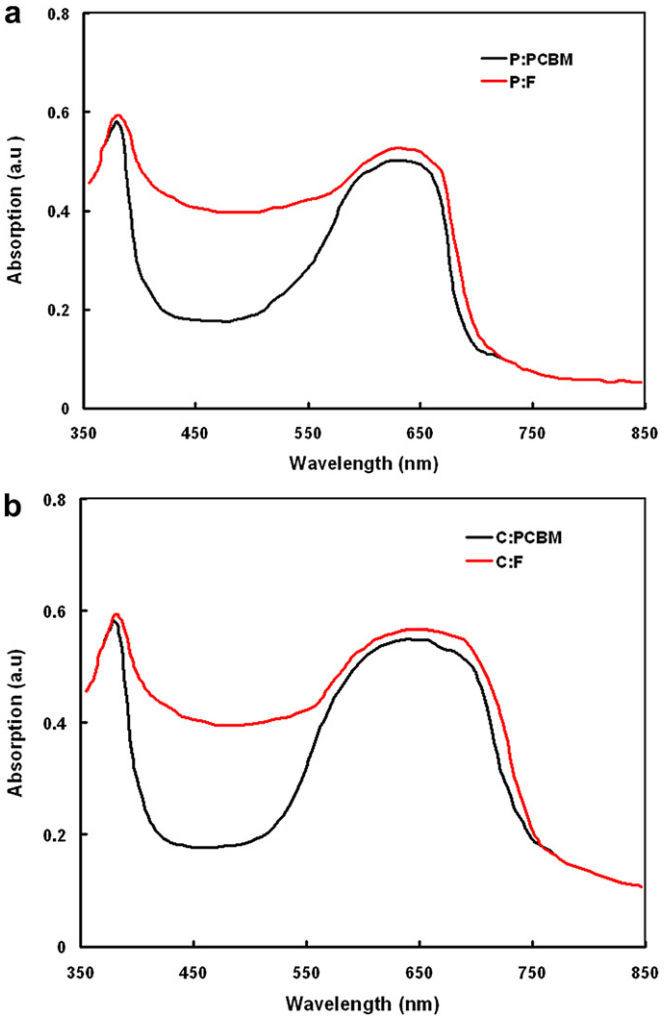

Fig. 8. Normalized absorption spectra of (a) **P**:PCBM and **P**:**F** and (b) **C**:PCBM and **C**:F blend in thin film form, cast from THF solvent.

Despite recent advances, PCE for the OSC still need to be improved for their successful commercialization. The challenge for improving the PCE of OSC is to optimize the interfacial area of the donor/acceptor materials and improve charge mobility within the active layer by increasing mesoscopic order and crystallinity. Throughout literature, significant advances in the enhancement of PCE of OSCs are achieved by improvement in morphology [28]. The PCE of OSCs based on BHJ system depends strongly on processing conditions [29] and can be improved by increasing the crystalline nature of conjugated polymer using various methods. The active BHJ active layer films used in the OSCs are usually fabricated by spin casting. A controlled thermal annealing step after active layer deposition has been introduced as a way to improve morphology of the BHJ layer and increase the quantum efficiency of the device [30]. An optimal phase separated morphology for maximum PCE is a non-equilibrium mixture with nanoscale phase separation and connectivity.

Since molecular order in both the electron donor and acceptor domains is an important factor for high PCE of the BHJ solar cell [31], researchers have also looked into alternatives to thermal treatment. Solvent annealing has been reported to enhance the PV performance of OSC based on BHJ active layer [32]. Excess solvent allows the components to remain partially dissolved and diffuse at a high rate to arrange into more energetically favorable ordered structure, thus increasing the crystallinity of the film. The use of

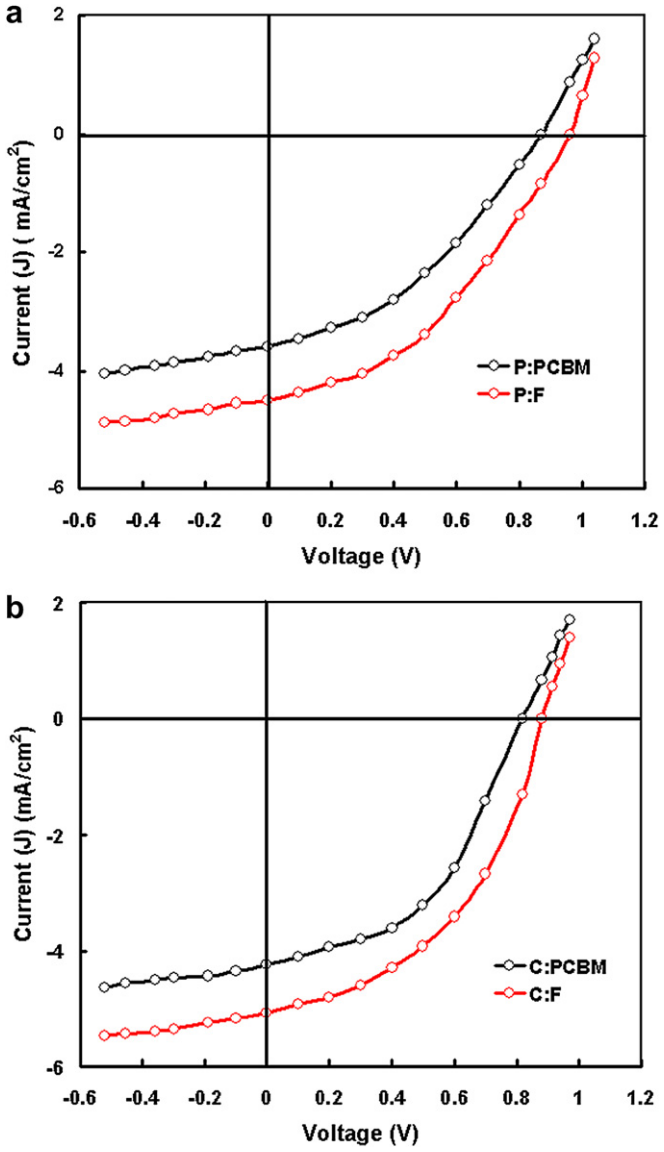

Fig. 9. Current –voltage characteristics of the BHJ photovoltaic devices based on (a) **P**:PCBM and **P**:**F** and (b) **C**:PCBM and **C**:**F** blends cast from THF solvent, under illumination intensity of 100 mW cm^{-2}.

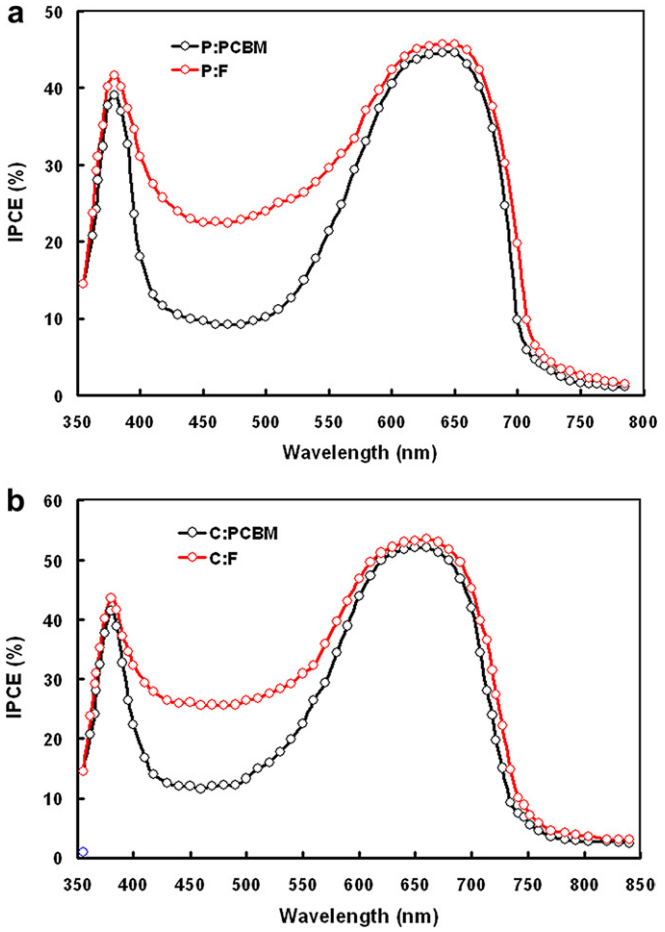

Fig. 10. IPCE spectra of BHJ photovoltaic devices based on (a) **P**:PCBM and **P**:**F** and (b) **C**:PCBM and **C**:**F** blends cast from THF solvent.

solvent additives during the processing the film also have been explored as a viable way to improve the morphology of BHJ active layer used in the polymer based solar cells [33]. From the manufacturing perspective, the advantage of solvent additives is that blend does not require additional processing steps and has been applied to polymers with both high and low solubility, and demonstrated to improve the performance of devices [34].

We have investigated the effect of mixed solvent on the photovoltaic response of the BHJ solar cells based on **P**:**F** and **C**:**F** blends. The J–V characteristics of the devices under illumination intensity were shown in Fig. 11(a) and the photovoltaic parameters were complied in the Table 2. When 2% of DIO (by volume) is added to the THF solution of the blend, the J_{sc} of the devices based on **P**:**F** and **C**:**F** blends reaches about 5.36 mA cm^{-2} and 7.0 mA cm^{-2}, respectively, which is almost 1.5 fold of the devices cast for THF solvent, resulting in over all PCE of 2.41% and 3.14%. This may be attributed to the enhanced crystalline nature of small molecule which not only enhances the optical absorption but also provides the improvement in hole transport due to the good connectively of small molecule with the anode. Fig. 11(b) shows the IPCE spectra of the devices based on **P**:**F** and **C**:**F** cast from DIO/THF solvent. In comparison with the IPCE spectrum of the devices based on THF solvent, the IPCE values of device based on DIO/THF solvent increased significantly in the wavelength region of 600–750 nm, which corresponds to the absorption of the **P** or **C**. This is due to the increased crystalline nature of the **P** or **C** in the blend as confirmed from the XRD data.

The optical absorption spectra of **P**:**F** and **C**:**F** blends in thin film form, cast from the mixed DIO/THF mixed solvent and are shown in Fig. 12. With the addition of DIO, the absorption peak corresponds to the small molecule (**P** or **C**) shifts towards longer wavelength region (red shift) and the intensity of absorption coefficient in longer wavelength region has also increased significantly. The vibronic shoulder peak in longer region is also observed in the optical absorption, when the film was cast from the DIO/THF solvent. The observed red shift corresponds to the **P** or **C** is attributed to the enhanced conjugation length and more ordered structure of **P** or **C** in the blend. The higher degree of crystallinity as indicated by a red shift in the absorption band and a clear appearance of shoulder in long wavelength region, which is due to the enhanced $\pi-\pi^*$ conjugation and an increased crystallinity nature of the blend. This observation has also been confirmed from the XRD data. Fig. 13(a) and (b) show the XRD pattern of the pristine **C** film and **C**:**F** blend film, respectively, cast from the THF and mixed DIO/THF solvent. The XRD band with a peak at $2\theta = 6.8^{\circ}$ was observed for **C** film cast from THF, corresponding to an interplanar distance of

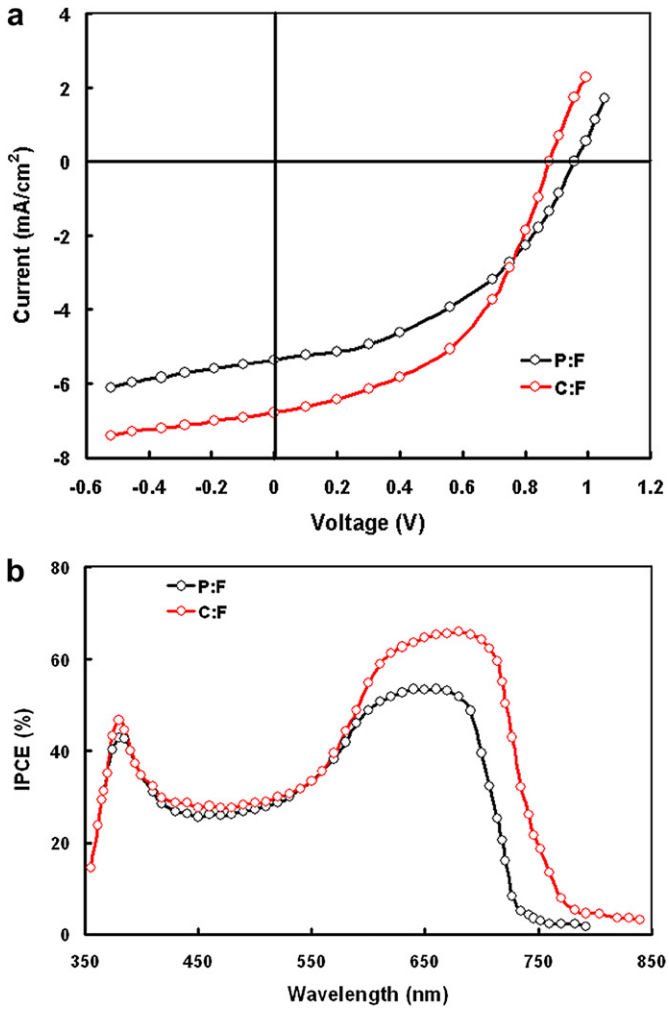

Fig. 11. (a) Current –voltage characteristics under illumination intensity of 100 mWcm^{-2} and (b) IPCE spectra of the BHJ photovoltaic devices based on **P**:**F** and **C**:**F** blends cast from mixed DIO/THF solvents.

14.5 Å. When the film is cast from DIO/THF solvent, this diffraction intensity was increased, indicating that the crystallinity of the pristine **C** film has been enhanced. It can be seen from the Fig. 12(b) that the when the **C**:**F** blend film casted from the THF solvent, the diffraction band become wider and the intensity of the peak becomes weak, suggesting an effective mixing of **C** with **F**, which interferes with the molecular packing of **C**. However, when the **C**:**F** blend cast from the DIO/THF solvent, the intensity of diffraction peak corresponding to $2\theta = 6.8^\circ$ increases. Since the boiling point of the DIO is higher than that of THF, the blend evaporates slowly that

Table 2
Photovoltaic parameters of the devices based on **P**:PCBM or **F** and **C**:PCBM or **F** blends cast from different solvents.

Blend	Short circuit current (J_{sc}) (mA/cm^2)	Open circuit voltage (V_{oc}) (V)	Fill factor (FF)	Power conversion efficiency (PCE) (%)
P:PCBM[a]	3.6	0.87	0.38	1.20
P:**F**[a]	4.5	0.96	0.44	1.90
C:PCBM[a]	4.24	0.82	0.42	1.46
C:**F**[a]	5.1	0.88	0.46	2.06
P:**F**[b]	5.36	0.94	0.48	2.41
C:**F**[b]	7.0	0.86	0.52	3.13

[a] cast from THF solvent.
[b] cast from mixed DIO/THF solvent.

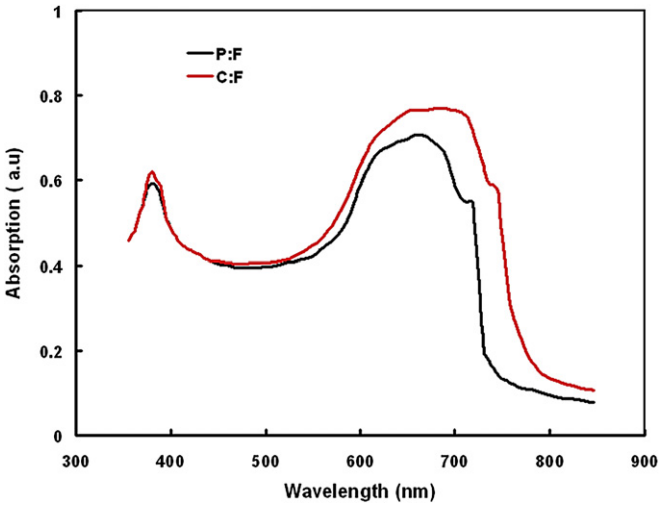

Fig. 12. Normalized absorption spectra of **P**:**F** and **C**:**F** blend in thin film form, cast from mixed solvent.

has resulted an increase in the crystallinity of the blend. The change in the film crystalline nature, when DIO is mixed with THF also agrees with the observed change in the absorption spectra. Highly ordered $\pi-\pi^*$ conjugation, has been described earlier, is known to improve the enhancement of the charge carrier mobility (particularly hole mobility) in the blend film [35].

We have measured the hole and electron mobility in the blends, fitting the J–V characteristics of hole only device ITO/PEDOT:PSS/**C**:**F**/Au and electron only device Al/**C**:**F**/Al with SCLC model (as described earlier). The measured value of the hole mobility is 8.8×10^{-6} cm^2 V^{-1} s^{-1} and 1.1×10^{-4} cm^2 V^{-1} s^{-1} for THF and DIO/THF cast films, respectively. However, the electron mobility is slightly enhanced i.e. 3.2×10^{-4} cm^2 V^{-1} s^{-1} and 7.6×10^{-4} cm^2 V^{-1} s^{-1} for THF and DIO/THF casted films, respectively. The smaller value of the ratio of electron and hole mobilities

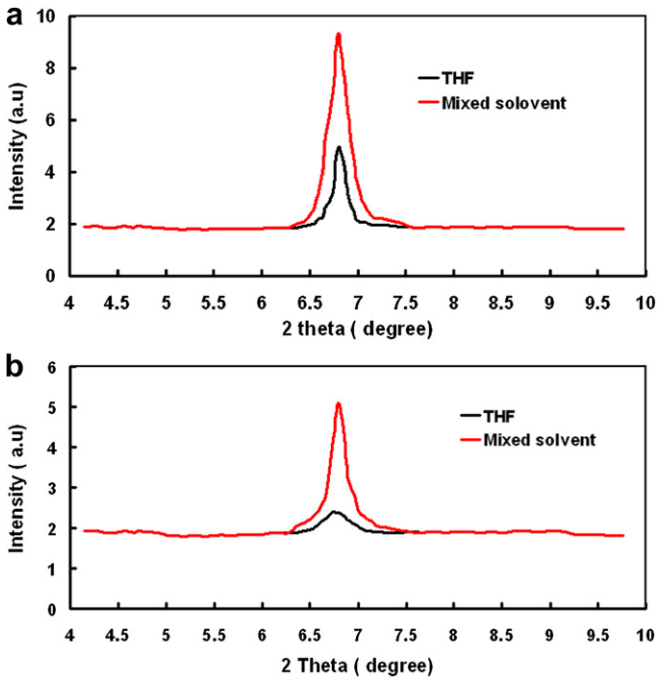

Fig. 13. XRD diffraction pattern of (a) pristine **C** thin films and (b) **C**:**F** blend cast from the THF and DIO/THF mixed solvent.

for DIO/THF cast film i e. 6.9 as compared to that for THF cast film i.e.36, indicates a more balanced charge transport, which results higher J_{sc} and PCE.

4. Conclusions

We have investigated the optical, electrochemical properties of two low band gap small molecules **P** and **C** having pyrrole and carbazole central donor units, respectively and same 2-(4-nitrophenyl) acrylonitrile acceptor segment, with an optical band gap 1.70 eV and 1.62 eV, respectively. The LUMO and HOMO levels were estimated from both DFT calculation as well as cyclic voltammetry and found that these values are suitable for the use of these small molecules as electron donor along with fullerene derivatives as electron acceptor for the fabrication of BHJ solar cells. The PCE of the BHJ organic solar cells based on **P**:PCBM and **C**:PCBM cast from the THF solvent is 1.20% and 1.46%, respectively. The higher PCE for the device based on **C** is attributed to the higher hole mobility in **C** as compared to **P**. The PCE for the devices based on **P**:**F** and **C**:**F** is 1.90% and 2.06%, respectively. The enhanced PCE for the devices based on **F** as electron acceptor in the BHJ active layer as compared to the PCBM as electron acceptor might be due to the strong absorption of **F** in visible region as compared to PCBM, resulting higher J_{sc} and also attributed to the higher LUMO level of **F** as compared to PCBM, improving V_{oc}. The PCE has been further improved up to 2.41% and 3.13% for the BHJ devices based on the **P**:**F** and **C**:**F** blends, respectively, cast from the DIO/THF mixed solvents. The improved PCE of the BHJ OSCs based on the blends cast from mixed DIO/THF solvent has been attributed to the improved charge transport in the device due to the increased crystalline nature of the blends.

References

[1] (a) Krebs FC. Polymer photovoltaics: a practical approach. Bellingham: SPIE; 2008;
(b) Moule AJ. Power from plastic. Curr Opin Solid State Mater Sci 2010;14:123–30;
(c) Hou J, Chen TL, Zhang S, Huo L, Sista S, Yang Y. An easy and effective method to modulate molecular energy levels of poly (3-alkylthiophene) for high voc polymer solar cells. Macromolecules 2010;42:9217–9;
(d) Krebs FC, Jorgensen M, Norman K, Hagemann O, Alstrup J, Nielsen TD, et al. A complete process for production of flexible area polymer solar cells entirely using screen printing – first public demonstration. Sol Energy Mater Sol Cells 2009;93:422–41;
(e) Coakley KM, McGhee MD. Conjugated polymer photovoltaic cells. Chem Mater 2004;16:4533–42;
(f) Krebs FC, Tromholt T, Jorgensen M. Up scaling of polymer solar cell fabrication using roll to roll processing. Nanoscale 2010;2:873–86;
(g) Krebs FC, Nieisen TD, Fyenbo J, Wadstrom M, Pedersen MS. Manufacture, integration and demonstration of polymer solar cells in a lamp for the "lighting Africa" initiative. Energy Environ Sci 2010;3:512–25;
(h) Gunes S, Neugebauer H, Sariciftci NS. Conjugated polymer based organic solar cells. Chem Rev 2007;107:1324–38;
(i) Chen JW, Cao Y. Development of novel conjugated donor polymers for high efficiency bulk heterojunction photovoltaic devices. Acc Chem Res 2009;42:1709–18;
(j) Cheng YJ, Yang SH, Hsu CS. Synthesis of conjugated polymers for organic solar cell applications. Chem Rev 2009;109:5868–923;
(k) Zhan XW, Zhu DB. Conjugated polymers for high efficiency organic photovoltaics. Polym Chem 2010;1:409–19;
(l) Krebs FC, Fyenbo J, Jorgensen M. Product integration of compact roll to roll processed polymer solar cell modules:method and manufacture using flexographic printing, slot die coating and rotary screen printing. J Mater Chem 2010;20:8994–9001.

[2] (a) Yu G, Heeger AJ. Charge separation and photovoltaic conversion in polymer composites with internal donor/acceptor heterojunctions. J Appl Phys 1995;78:4510–5;
(b) Yu G, Gao J, Hummelen JC, Wudl F, Heeger AJ. Polymer photovoltaic cells: enhanced efficiencies via a network of internal donor–acceptor heterojunctions. Science 1995;270:1789–91.

[3] (a) Blom PWM, Mihailetchi VD, Koster LJA, Markov DE. Device physics of polymer:fullerene bulk Heterojunction solar cells. Adv Mater 2007;19:1551–6;
(b) Chen LM, Hong Z, Li G, Yang Y. Recent progress in polymer solar cells: manipulation of polymer:fullerene morphology and the formation of efficient inverted polymer solar cells. Adv Mater 2009;21:1434–49;
(c) Thompson BC, Frechet JMJ. Polymer–fullerene composite solar cells. Angew Chem Int Ed 2008;47:58–77.

[4] (a) Ma WL, Yang CY, Gong X, Lee K, Heeger AJ. Thermally stable, efficient polymer solar cells with nanoscale control of the interpenetrating network morphology. Adv Funct Mater 2005;15:1617–22;
(b) Kim Y, Cook S, Tuladhar SM, Choulis SA, Nelson J, Durrant JR, et al. A strong regioregularity effect in self-organizing conjugated polymer films and high-efficiency polythiophene:fullerene solar cells. Nat Mater 2006;5:197–203;
(c) Li G, Shrotriya V, Huang J, Yao Y, Moriarty T, Emery K, et al. High-efficiency solution processable polymer photovoltaic cells by self-organization of polymer blends. Nat Mater 2005;4:864–8;
(d) Reyes-Reyes M, Kim K, Carroll DL. High-efficiency photovoltaic devices based on annealed poly(3-hexylthiophene) and 1-(3-methoxycarbonyl)-propyl-1- phenyl-(6,6)C_{61} blends. Appl Phys Lett 2005;87:083506.

[5] (a) Liang Y, Xu Z, Xia J, Tsai ST, Wu Y, Li G, et al. For the bright future-bulk heterojunction polymer solar cells with power conversion efficiency of 7.4%. Adv Mater 2010;22:E135–8;
(b) Chen HY, Hou J, Zhang S, Liang Y, Yang G, Yang Y, et al. Polymer solar cells with enhanced open-circuit voltage and efficiency. Nat Photonics 2009;3:649–53;
(c) Peet J, Kim JY, Coates NE, Ma WL, Moses D, Heeger AJ, et al. Efficiency enhancement in low-bandgap polymer solar cells by processing with alkane dithiols. Nat Mater 2007;6:497–500;
(d) Park SH, Roy A, Beaupre S, Cho S, Coates N, Moon JS, et al. Bulk heterojunction solar cells with internal quantum efficiency approaching 100%. Nat Photonics 2009;3:297–302;
(e) Liang Y, Wu Y, Feng D, Tsai ST, Son HJ, Li G, et al. Development of new semiconducting polymers for high performance solar cells. J Am Chem Soc 2009;131:56–7;
(f) Chen YC, Yu CY, Fan YL, Hung LI, Chen CP, Ting C. Low band gap conjugated polymer for high efficient photovoltaic applications. Chem Commun 2010;46:6503–5;
(g) Chu TY, Lu J, Beaupre S, Zhang Y, Pouliot JR, Wakim S, et al. Bulk heterojunction solar cells using thieno[3,4-c]pyrrole-4,6-dione and dithieno[3,2-*b*:2′,3′-d]silole copolymer with a power conversion efficiency of 7.3%. J Am Chem Soc 2011;133:4250–3;
(h) Price SC, Stuart AC, Yang L, Zhou H, You W. Fluorine substituted conjugated polymer of medium band Gap yields 7% efficiency in polymer: fullerene solar cells. J Am Chem Soc 2011;133:4625–31.

[6] Solarmer Energy Inc. Solarmer Energy Inc breaks psychological barrier with 8.13 % OPV efficiency. Press release retrieved from, http://www.Business.com/news/home/20100727005484; July 27, 2010.

[7] (a) Scharber MC, Muhlbacher D, Koppe M, Denk P, Waldauf C, Heeger AJ, et al. Design rules for donors in bulk heterojunction solar cells –towards 10 % conversion efficiency. Adv Mater 2006;18:789–94;
(b) Chen HY, Hou JH, Zhang SQ, Liang YY, Yang GW, Yang Y, et al. Polymer solar cells with enhanced open circuit voltage and efficiency. Nat Photonics 2009;3:649–53.

[8] Moet DJD, Lenes M, Kotlarski JD, Veenstra SC, Sweelssen J, Koetse MM, et al. Impact of molecular weight on charge carrier dissociation in solar cells from polyfluorene derivative. Org Electron 2009;10:1275–81.

[9] (a) Lloyd MT, Anthony JE, Malliaras GG. Photovoltaic from small molecules. Mater Today 2009;10:34–41;
(b) Roncali J. Molecular bulk heterojunction: an emerging approach to organic solar cells. Acc Chem Res 2009;42:1719–30;
(c) Walker B, Kim C, Nguyen TQ. Small molecule solution processed bulk heterojunction solar cells. Chem Mater 2010;23:470–82.

[10] (a) Xue JU, Chida S, Rand BP, Forrest SR. Asymmetric tandem organic photovoltaic cells with hybrid planar–mixed molecular heterojunctions. Appl Phys Lett 2004;85:5757–9;
(b) Chan MY, Lai SL, Fung MK, Lee CS. Doping induced enhancement in organic photovoltaic devices. Appl Phys Lett 2007;90:023504–6;
(c) Xue JG, Rand BP, Uchida S, Forrest SR. A hybrid planar–mixed molecular heterojunction photovoltaic cells. Adv Mater 2005;17:66–71.

[11] (a) Ma CQ, Mena-Osteritz E, Debaerdemaeker T, Wienk MM, Janssen RAJ, Bauerle P. Functionalized 3D oligothiophene dendrons and dendrimers – novel macromolecules for organic electronics. Angew Chem Int Ed 2007;46:1679–83;
(b) Ma CQ, Fonrodona M, Schikora MC, Wienk MM, Janssen RAJ, Bauerle P. Solution processed bulk heterojunction solar cells based on monodisperse dendritic oligothiophenes. Adv Funct Mater 2008;18:3323–31;
(c) Ma WWH, Wong CQ, Pisula W, Yan C, Feng XL, Jones DJ, et al. Self assembling thiophenes dendrimers with a hexa-peri hexabenocoronene-synthesis, characterization and performance in bulk heterojunction solar cells. Chem Mater 2010;22:457–66;
(d) Yin B, Yang L, Li Y, Chen Y, Qi Q, Zhang F, et al. Solution processed bulk heterojunction organic solar cells based on an oligothiophene derivatives. Appl Phys Lett 2010;97:023303.

[12] (a) Sun X, Zhou Y, Wu W, Liu Y, Tian W, Yu G, et al. X-shaped oligothiophenes as a new class of electron donors for bulk heterojunction solar cells. J Phys Chem B 2006;110:7702–7;
(b) Roquet S, Cravino A, Leriche P, Aleveque O, Frere P, Roncali J.

Triphenylamine – theinylenevinylene hybrid systems with internal charge transfer as donor materials for solar cells. J Am Chem Soc 2006;28:3459–66;
(c) He C, He QG, Yi YP, Wu GL, Bai FL, Shuai ZG, et al. Improving the efficiency of solution processable organic photovoltaic devices by star shaped molecular geometry. J Mater Chem 2008;18:4085–90;
(d) Li WW, Du C, Li FH, Zhou Y, Fahiman M, Bo ZS, et al. Benzothiadiazole based linear and star molecules: design, synthesis and their application in bulk heterojunction organic solar cells. Chem Mater 2009;21:5327–34;
(e) Zhang J, Yang Y, He C, He YJ, Zhao GJ, Li YF. Solution processable star shaped photovoltaic organic molecule with triphenylamine core and benzothiadiazole – thiophene arms. Macromolecules 2009;42:7619–22;
(f) Shang H, Fan H, Liu Y, Hu W, Li Y, Zhan X. A solution processable star shaped molecule for high performance organic solar cells. Adv Mater 2011;23:1554–7.

[13] (a) Lincker F, Delosc Bailly N, Bailly S, De Bettignes R, Billon M, Pron A, et al. Fluorenone based molecule for bulk heterojunction solar cells: synthesis, characterization and photovoltaic properties. Adv Funct Mater 2008;18:3444–53;
(b) Tomayo AB, Dang XD, Walker B, Seo J, Kent T, Nguyen TQ. High performance solution-processed bulk heterojunction solar cells based on diketopyrrolopyrrolo derivative/C_{70} blends. Appl Phys Lett 2009;19:103301;
(c) Walker B, Tamayo AB, Dang XD, Zalar P, Seo JH, Garcia A, et al. Nanoscale phase separation and high photovoltaic efficiency in solution-processed, small-molecule bulk heterojunction solar cells. Adv Funct Mater 2009;19:3063–9;
(d) Liu Y, Wan X, Yin B, Zhou J, Long G, Yin S, et al. Efficient solution processed bulk-heterojunction solar cells based a donor–acceptor oligothiophene. J Mater Chem 2010;20:2464–8;
(e) Zhao X, Piliego C, Kim B, Poulsen DA, Ma B, Unruh DA, et al. Solution processable crystalline platinum acetylide oligomers with broadband absorption for photovoltaic cells. Chem Mater 2010;22:2325–32;
(f) Tamayo A, Kent T, Tantitiwat M, Dante MA, Rogers J, Nguyen TQ. Influence of alkyl substituents and thermal annealing on the film morphology and performance of solution processed, diketopyrrolopyrrole-based bulk heterojunction solar cells. Energy Environ Sci 2009;2:1180–6;
(g) Zhang J, Wu G, He C, Deng D, Li Y. Tripheylamine containing D-A.D molecules with dicyanomethylene) pyran as acceptor unit for bulk heterojunction organic solar cells. J Mater Chem 2011;21:3768–74.

[14] (a) Wei G, Wang Renshaw SK, Thompson ME, Forrest SR. Solution processed squaraine bulk heterojunction photovoltaic cells. ACS Nano 2010;4:1927–34;
(b) Ning Z, Tian H. Triarylamine: a promising core unit for efficient photovoltaic materials. Chem Commun; 2009:5483–95;
(c) Burckstummer H, Kronenber NM, Gsanger K, Stolte M, Meerholz K, Wurthner F. Tailored merocyanine dyes for solution processed BHJ solar cells. J Mater Chem 2010;20:240–3.

[15] Mikroyannidis JA, Kabanakis A, Tsagkournos D, Balraju P, Sharma GD. Bulk heterojunction solar cells based on a low band gap soluble bisazopyrrole and the corresponding BF_2-azopyrrole complex. J Mater Chem 2010;20:6464–71.

[16] Mikroyannidis JA, Tsagkournos DV, Sharma SS, Kumar A, Vijay YK, Sharma GD. Effective bulk heterojunction solar cells based on low band gap bisazo dyes containing anthracene and/or pyrrole. Sol Energy Mater Sol Cells 2010;94:2318–27.

[17] Mikroyannidis JA, Kabanakis AN, Balraju P, Sharma GD. Bulk heterojunction photovoltaics using broadly absorbing small molecules based on 2-styryl-5-phenylazo-pyrrole. Langmuir 2010;26:17739–48.

[18] Mikroyannidis JA, Kabanakis AN, Sharma SS, Sharma GD. A simple Effective modification of PCBM for use as an electron acceptor in efficient bulk heterojunction solar cells. Adv Funct Mater 2011;21:746–55.

[19] Frisch MJ, Trucks GW, Schlegel HB, Scuseria GE, Robb MA, Cheeseman JR, et al. Gaussian 09, Revision A.02. Wallingford CT: Gaussian, Inc; 2009.

[20] (a) Kohn W, Sham LJ. Self-consistent equations including exchange and correlation effects. Phys Rev 1965;140:A1133–8;
(b) Parr RG, Yang W. Density-functional theory of atoms and molecules. Oxford: Oxford University Press; 1989.

[21] (a) Becke AD. Density-functional thermochemistry – III. The role of exact exchange. J Chem Phys 1993;98:5648–52;
(b) Lee C, Yang W, Parr RG. Phys Rev B 1988;37:785–9.

[22] Furche F, Ahlrichs R. J Chem Phys 2002;117:7433–47.

[23] Tomasi T, Mennucci B, Cammi R. Chem Rev 2005;105:2999–3093.

[24] (a) Gorelsky SI. SWizard program. Ottawa, Canada: University of Ottawa, http://www.sg-chem.net/; 2010;
(b) Gorelsky SI, Lever ABP. Electronic Structure and spectra of ruthenium diimine complexes by density functional theory and INDO/S. Comparison of the two methods. J Organomet Chem 2001;635:187–96.

[25] (a) Li Y, Cao Y, Gao J, Wang D, Yu G, Heeger AJ. Electrochemical properties of luminescent polymers and light emitting electrochemical cells. Synth Met 1999;99:243–8;
(b) Sun QJ, Wang HQ, Yang CH, Li YF. Synthesis and electroluminescence of novel copolymers containing crown ether spacer. J Mater Chem 2003;13:800–6.

[26] Chen C, Chan S, Chan T, Ting C, Ko B. Low-band gap poly(thiophene-phenylene-thiophene) derivatives with broaden absorption spectra for use in high-performance bulk-heterojunction polymer solar cells. J Am Chem Soc 2008;130:12828–33.

[27] (a) Chirvase D, Chiguvare Z, Knipper M, Parisi J, Dyakonov Y, Hummelen JC. Temperature dependent characteristics of P3HT-fullerene based bulk heterojunction organic solar cells. J Appl Phys 2003;93:3376–84;
(b) Malliaras GG, Salem JR, Brock PJ, Scott C. Electrical characteristics and efficiency of single layer organic light emitting diodes. Phys Rev B 1998;58:R13411–4.

[28] (a) Li G, Shrotriya V, Huang J, Yao Y, Moriarty T, Emery K, et al. High efficiency solution processable polymer photovoltaic cells by self organization of polymer blends. Nat Mater 2005;4:864–8;
(b) Ma W, Yang C, Gong X, Lee K, Heeger AJ. Thermally stable, efficient polymer solar cells with nanoscale control of the interpenetrating network morphology. Adv Funct Mater 2005;5:1617–22;
(c) Padinger F, Rittberger RS, Sariciftci NS. Effect of post production treatment on plastic solar cells. Adv Funct Mater 2003;13:85–8.

[29] (a) Hoppe H, Sariciftci NS. Morphology of polymer/fullerene bulk heterojunction solar cells. J Mater Chem 2006;16:45–61;
(b) Yang X, Loos J. Towards high performance polymer solar cells: the importance of morphology control. Macromolecules 2007;40:1353–62.

[30] Ma WL, Yang CY, Gong X, Lee K, Heeger AJ. Thermally stable, efficient polymer solar cells with nanoscale control of the interpenetrating network morphology. Adv Funct Mater 2005;15:1617–22.

[31] (a) Chirvase D, Parisi J, Hummelen JC, Dyakonov V. Influence of nanomorphology on the photovoltaic action of polymer:fullerene composites. Nanotechnology 2004;15:1317–23;
(b) Savenije TJ, Kroeze JE, Yang XN, Loos J. The effect of thermal treatment on the morphology and charge transfer dynamics in a polythiophene – fullerene bulk heterojunction. Adv Funct Mater 2005;15:1260–6;
(c) Zhokhavets U, Erb T, Gobsch G, Al-Ibrahim M, Ambacher O. Relation between absorption and crystallinity of P3HT – fullerene films for plastic solar cells. Chem Phys Lett 2006;418:347–50.

[32] (a) Li G, Yao Y, Yang H, Shrotriya V, Yang G, Yang Y. Solvent annealing effect in polymer solar cell based on poly (3–hexylthiophene) and methanofullerenes. Adv Funct Mater 2007;17:1636–44;
(b) Shrotriya V, Yao Y, Li G, Yang Y. Effect of self-organization in polymer/fullerene bulk heterojunctions on solar cells performance. Appl Phys Lett 2006;89:063505;
(c) Li G, Shrotriya V, Yao Y, Huang JS, Yang Y. Manipulating regioregular poly (3-hexylthiophene):PCBM blends-routes towards high efficiency polymer solar cells. J Mater Chem 2007;17:3126–40.

[33] (a) Peet J, Kim JY, Coates NE, Ma WL, Moses D, Heeger AJ, et al. Efficiency enhancement in low band gap polymer solar cells by processing with alkane dithiols. Nat Mater 2007;6:497–500;
(b) Lee JK, Ma WL, Brabec CJ, Yuen J, Moon JS, Kim JY, et al. Procesing additives for improved efficiency from bulk heterojunction solar cells. J Am Chem Soc 2008;130:3619–23;
(c) Moon JS, Takacs CJ, Cho S, Coffin RC, Kim H, Bazan GC, et al. Effect of processing additive on the nanomorphology of a bulk heterojunction materials. Nano Lett 2010;10:4005–10;
(d) Coffin RC, Peet J, Roger J, Bazan GC. Streamlined microwave assisted preparation of narrow band gap conjugated polymers for high perfromance bulk heterojunction soalr cells. Nat Chem 2009;1:657–61;
(e) Peet J, Soci C, Coffin RC, Nguyen TQ, Mikhallovsky A, Moses D, et al. Method for increasing the photoconductive response in conjugated polymer/fullerene composites. Appl Phys Lett 2006;89:252105;
(f) Moet DJD, Lenes M, Morana M, Azimi H, Brabec CJ, Blom PWM. Enhanced dissociation of charge transfer states in narrow band gap polymer: fullerene soalr cells processed with 1,8 octanedithiol. Appl Phys Lett 2010;96:213506.

[34] Chen HY, Hou JH, Zhang SQ, Liang YY, Yang GW, Yang Y, et al. Polymer solar cells with enhanced open circuit voltage and efficiency. Nat Photon 2009;3:649–53.

[35] (a) Park JH, Kim JS, Lee JH, Lee WH, Cho K. Effect of annealing solvent solubility on the performance of poly (3-hexylthiophene)/methanofullerene solar cells. J Phys Chem C 2009;113:17579–175584;
(b) Yang X, Loos J, Veenstra SC, Verhees WJH, Wienk MM, Kroons JM, et al. Nanoscale morphology of high performance polymer solar cells. Nano Lett 2005;5:579–83;
(c) Mikroyannidis JA, Tsagkournos DV, Sharma SS, Vijay YK, Sharma GD. Bulk heterojunction photovoltaics using broadly absorbing small molecules based on 2-styryl-5-phenylazo-pyrrole. J Mater Chem 2011;21:4679–88.